Tellus (1985), 37A, 156–162

Mesoscale circulations in a hydrostatic model: coastal convergence and orographic lifting

By MIKKO ALESTALO, *Finnish Meteorological Institute, Vuorikatu 24, 00100 Helsinki 10, Finland* and HANNU SAVIJÄRVI, *Department of Meteorology, University of Helsinki, Hallituskatu 11–13, 00100 Helsinki 10, Finland*

(Manuscript received December 16, 1983; in final form August 10, 1984)

ABSTRACT

A hydrostatic two-dimensional K-theory model ($\Delta x = 4$ km, 10 σ levels) is described and used to simulate mesoscale circulations developing in a neutral atmospheric boundary layer when wind blows over or along a 80 km wide sea gulf. On-shore geostrophic wind of 10 m s^{-1} induces rising motion ~1 cm/s at 300 m level above the coastline due to roughness difference (coastal convergence) and ~1.6 cm s^{-1} further inland over sloping land (orographic lifting). Off-shore wind produces sinking motion. When the geostrophic wind 10 m s^{-1} blows along the coastline with lower pressure over the sea, the coastal convergence induces rising motion ~0·5 cm s^{-1} 25 km off-shore at 600 m level, weak sinking motion just over the coastline below 200 m, and the topography induces sinking motion further inland. The results are opposite for reversed wind direction. The two effects are additive.

1. Introduction

Near the coastlines, the observed cloudiness and precipitation is often larger than further inland, depending, however, on the wind direction. For instance, Solantie (1975) studied the observed precipitation from October to April on all Finnish stations and found that "during winds blowing onto land, the combined orographic and coastal effect increases the precipitation by 40% in a zone 20 km inland from the coast. Further inland, in places where the earth slopes upward at a rate of 10 m per 10 km, the slope effect increases the precipitation by 20%". Solantie also classified wind directions during rainy periods finding that on-shore and low-over-sea winds were predominant. These wind directions were also characterized by large radar reflectivities during summer nights (when thermal effects are small) in Heikinheimo and Puhakka (1980). Radar observations (Browning, 1980) indicate that the increase in the rainfall rate near the coasts is largest in the lowest km.

The reason for the variable local precipitation on the coast in the absence of thermal forcing lies in the vertical velocities induced by roughness change and forced lifting over the sloping land. Both effects are described qualitatively in textbooks and are included in large scale and mesoscale numerical models. However, we have not found any systematic published results of the mesoscale vertical velocity patterns and magnitudes caused by them as a function of wind direction.

This article describes the vertical velocity patterns induced by geostrophic flow over a sloping, rough coast in a high resolution mesoscale model. The flow is neutral and barotropic and there are no heating contrasts, so the resulting mesoscale circulation due to mechanical (shear) turbulence is in a quasi-steady state. The model framework is an 80 km wide sea surrounded by 85 km wide coasts rising up to 80 m. This simulates a cross-section through, e.g. the gulfs of the Baltic Sea or the great lakes of North America.

The hydrostatic model (10 levels, 4 km grid, Alpert et al. (1982)) is based on K-theory and is two-dimensional. Comparison is also made with an Ekman–Taylor (constant K)-type wind profile.

2. The model

The model is an improved version of that described in Alpert et al. (1982) where it was used to simulate wind structure over the Jordan Valley. The model has also been used in a study of Lake Michigan land breezes (Alpert and Neumann, 1983). Modifications have been made here to the surface layer formulation, stability dependence of diffusion coefficients and to the numerical scheme. Latitude 60° N is assumed.

The model is hydrostatic in a terrain-following (x, σ) coordinate system. It assumes a steady large-scale pressure gradient in the form of a background geostrophic wind which is constant in height (barotropic flow) in the present experiments. The model equations are as follows:

$$\frac{\partial u}{\partial t} = -u\frac{\partial u}{\partial x} - \dot{\sigma}\frac{\partial u}{\partial \sigma} + f(v - v_g) \tag{1a}$$

$$-RT/(p_* + p_t/\sigma)\frac{\partial p_*}{\partial x} - \frac{\partial \phi}{\partial x} + F_x,$$

$$\frac{\partial v}{\partial t} = -u\frac{\partial v}{\partial x} - \dot{\sigma}\frac{\partial v}{\partial \sigma} - f(u - u_g) + F_y, \tag{1b}$$

$$\frac{\partial \phi}{\partial (T/\theta)} = -c_p\,\theta, \tag{1c}$$

$$\frac{\partial \theta}{\partial t} = -u\frac{\partial \theta}{\partial x} - \dot{\sigma}\frac{\partial \theta}{\partial \sigma} + F_\theta, \tag{1d}$$

$$\frac{\partial p_*}{\partial t} = -\frac{\partial}{\partial x}(p_*u) - \frac{\partial}{\partial \sigma}(p_*\sigma), \tag{1e}$$

$$\frac{\partial p_*}{\partial t} = -\int_0^1 \frac{\partial (p_* u)}{\partial x}\,d\sigma, \tag{1f}$$

where

$$\sigma = (p - p_t)/(p_s - p_t) = (p - p_t)/p_*,$$

$$p_* = p_s - p_t,$$

and the symbols are standard. F_x, F_y and F_θ are the expressions for the change of momentum and potential temperature due to vertical diffusion. They are given, following K-theory, by

$$F_x = \frac{g^2}{p_*^2}\frac{\partial}{\partial \sigma}\left(\rho^2 K_z \frac{\partial u}{\partial \sigma}\right) \tag{2a}$$

$$F_y = \frac{g^2}{p_*^2}\frac{\partial}{\partial \sigma}\left(\rho^2 K_z \frac{\partial v}{\partial \sigma}\right) \tag{2b}$$

$$F_\theta = \frac{g^2}{p_*^2}\frac{\partial}{\partial \sigma}\left(\rho^2 K_z \frac{\partial \theta}{\partial \sigma}\right). \tag{2c}$$

The boundary conditions are $\dot{\sigma} = 0$ at $\sigma = 1$ ($p = p_s = 1013$ mb at sea level) and $\dot{\sigma} = 0$ at $\sigma = 0$ ($p = p_t = 763$ mb). Near the surface $u = v = 0$ at $z = z_0$. The roughness length z_0, topography and surface temperature are specified. Turbulent fluxes vanish at the upper boundary and all horizontal gradients vanish at the vertical boundaries.

The vertical turbulent transfer is determined through turbulent diffusivity coefficients K_z. They are defined using the classical mixing length concept (e.g. Blackadar, 1978)

$$K_z = l^2 S f(\mathrm{Ri}), \tag{3}$$

where l is the mixing length, S the wind shear,

$$S = \left[\left(\frac{\partial u}{\partial z}\right)^2 + \left(\frac{\partial v}{\partial z}\right)^2\right]^{1/2}, \tag{4}$$

and Ri the Richardson number,

$$\mathrm{Ri} = \frac{g}{\theta}\frac{\partial \theta/\partial z}{S^2}. \tag{5}$$

The mixing length is given by (Blackadar, 1962):

$$l = kz/(1 + kz/\lambda), \tag{6}$$

where k (the von Kármán constant) $= 0.4$ and $\lambda = 40$ m. The form chosen for the function $f(\mathrm{Ri})$ is:

$$f(\mathrm{Ri}) = (1 - 18\mathrm{Ri})^{1/2} \quad \text{for} \quad \mathrm{Ri} \leqslant 0 \tag{7a}$$

$$f(\mathrm{Ri}) = \exp(-2.3\mathrm{Ri}) \qquad \mathrm{Ri} > 0. \tag{7b}$$

In the present experiments, ABL is neutral and thus $f(\mathrm{Ri}) \simeq 1$ for all time.

For the lowest layer, $z = 10$ m, K_z is given by

$$K_z = \left(\frac{k}{\ln(z/z_0)}\right)^2 z\,|V|\,f(\mathrm{Ri}). \tag{8}$$

When combined with the vertical finite difference (backward) scheme for F_x, F_y in the lowest layer, the result is the classical drag law for the surface fluxes, where the stability dependence $f(\mathrm{Ri})$ is given by Monin–Obukov similarity theory and specified above.

The formulation of K_z at the lowest layer is slightly different to Alpert et al. (1982), where the effect of roughness is underestimated and the stability dependence ignored.

The horizontal grid length is 4 km. The 65 grid point area is such that there is an 80 km wide sea in the middle and 85 km of land on both sides. There are 10 levels in the vertical at the approximate heights of 10, 19, 33, 60, 110, 190, 330, 600, 1100 and 1900 m above the ground. The numerical scheme is based on Marchuk splitting.

The pressure gradient force is calculated on pressure levels to avoid large errors near steep topography. Vertical diffusion is calculated in a semi-implicit fashion and horizontal advection is based on cubic spline interpolation. Instead of explicit horizontal diffusion, a highly selective horizontal low-pass filter is applied to all fields. The filter eliminates $2\Delta x$ waves completely and is effective in removing reflected gravity waves.

The time integrations are started from neutral conditions (surface air temperature = 17 °C, $\partial T/\partial z = -9.7$ °C/km) with constant geostrophic wind 10 m/s either along or across the coastline. The initial wind is an Ekman-Taylor profile ($K = 5$ m^2 s^{-1}; $\varphi = 60°$N; $\alpha = 30°$ over land, 20° over sea); this gives quick damping of the initial inertial oscillation towards a quasi-steady state in about 4 h. The results are shown for 8 h after start using an 8 s time-step.

3. Results

The initial Ekman–Taylor wind hodograph (with $K_z = 5$ m^2 s^{-1} over land) and the steady state hodographs of the model over flat land and sea ($z_0 = 10$ cm and 1 mm, respectively) are shown in Fig. 1 for $V_g = (10, 0)$ m s^{-1}. Compared with

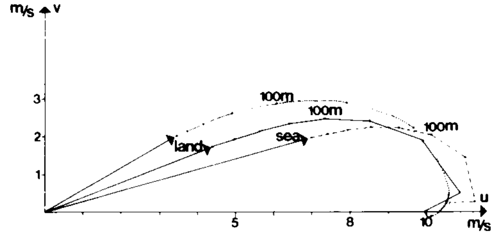

Fig. 1. Wind hodograph and 10 m wind vectors for the Ekman–Taylor spiral (dotted line) and for the model at quasi-steady state over land and sea. $u_g = 10$ m s^{-1}.

constant K_z case, the model (in which the vertical mean of K_z is 5 m^2 s^{-1} and maximum 8 m^2 s^{-1} at 300 m) gives a larger u-component and a smaller (cross-isobar) v-component. This is also seen in Fig. 2, where the $u(z)$ and $v(z)$ profiles are drawn both for the model and for the Ekman–Taylor spiral.

The difference between the wind component perpendicular to the coast, over land and sea will produce horizontal convergence or divergence and this leads to vertical motions. The coastal convergence is often quoted qualitatively in the climatological literature, but we have not found quantitative model simulations reported. Assuming an incompressible ABL, vertical integration of the Ekman–Taylor profile gives $w \sim 3$ cm s^{-1} as a first approximation, using realistic parameter values.

3.1. Geostrophic wind across the coastline

Fig. 3 shows the vertical motion field in the model when the geostrophic wind 10 m/s is across the coastlines (off-shore wind on the right, on-shore wind on the left coast in Fig. 3). The topography is flat and $z_0 = 10$ cm over land, 1 mm over sea. The greater wind speed over the sea produces divergence and sinking motion ($w = -1.2$ cm s^{-1} at 300 m level) over the lee coastline and convergence with rising motion ($w = 1.3$ cm/s) at the windward coastline. The two vertical velocity patterns are almost identical except for sign.

The vertical velocity patterns near the surface downwind from the roughness discontinuities (the coastlines) indicate an internal boundary layer (IBL) development. This is shown in more conventional terms in Fig. 4 where the $u(z)$ profiles have been plotted at grid points 0, 4, 8, 20 and 40 km downwind from the roughness change. The adaptation to a new surface stress value (0.21 N/m^2 over land, 0.10 over sea) infiltrates upward logarithmically; the depth of the IBL is roughly $\frac{1}{10}$ of the distance downwind for small distances. These results are in accordance with, e.g., Taylor (1969).

In the next experiment, the roughness is the same ($z_0 = 10$ cm) everywhere but the topography z_s of the land areas is introduced such that 80 km inland, z_s is 80 m above the sea level and the maximum slopes occur 40 km inland and are $1.5 \cdot 10^{-3}$ at both sides. These rather gentle slopes simulate those, e.g., across southern Finland and northern Estonia.

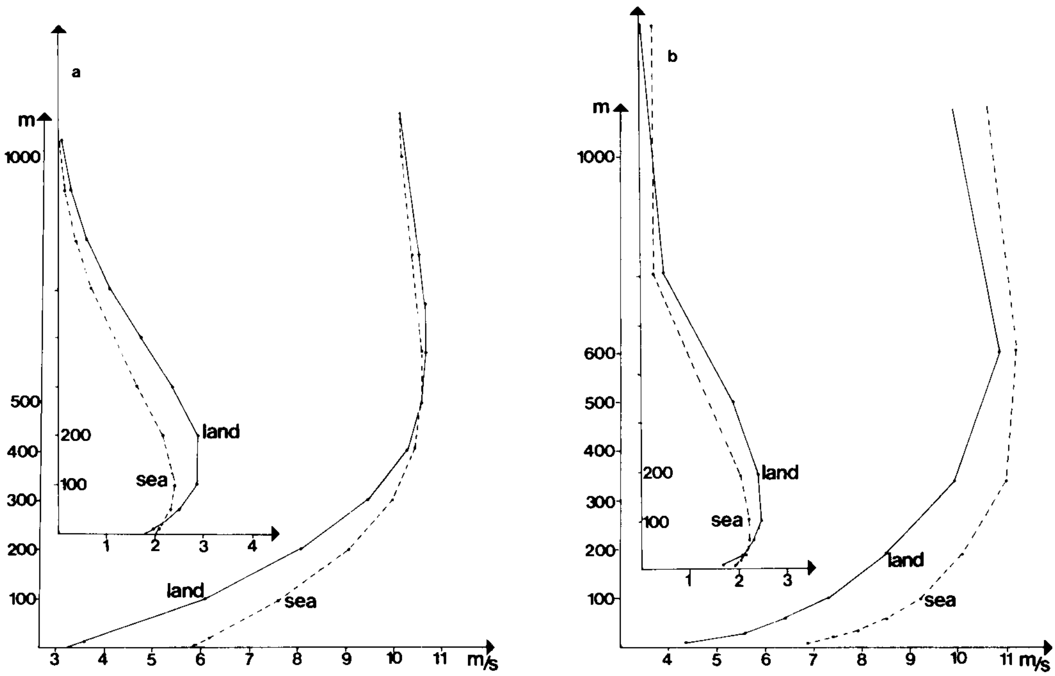

Fig. 2. The wind profiles $u(z)$ (in the main frame) and $v(z)$ (in the intake) at 60° N for $u_g = 10$ m s^{-1}, $v_g = 0$. (a) Ekman–Taylor solution when $K = 5$ m^2 s^{-1} and cross-isobar angle 30° over land, 20° over sea. (b) The model result at quasi-steady state.

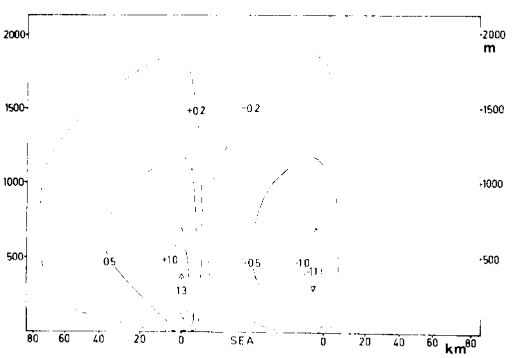

Fig. 3. Vertical velocity w (cm s^{-1}) at the steady state of the model with flat land, for geostrophic wind $u_g = 10$ m s^{-1}, $v_g = 0$ (from right to left).

The vertical velocities (not shown) induced by a geostrophic wind 10 m s^{-1} blowing across the hills are $w = -1.3$ cm s^{-1} down the slope at 600 m level and $w = 1.4$ cm s^{-1} at the uphill wind side over the maximum slopes. Combining the two effects in the model (smooth sea, rough, sloping coasts) gives the vertical velocity field in Fig. 5a. It is effectively the superposition of the coastal convergence (from Fig. 3) and orographic lifting patterns. The two effects are thus additive at low wind speeds and generate comparative vertical velocities for the parameter values in our experiments.

Numerical models are usually sensitive to the skin friction. Fig. 5b shows the vertical velocity in the present model when z_0 over land is increased from 10 cm (typical of farmland with few trees) to 70 cm (typical of forests with small hills). The increase in the land surface roughness intensifies the coastal convergence such that the w-extrema become -2.0 cm s^{-1} and 2.6 cm s^{-1} over the lee and windward coasts, respectively. These are about double as large as with $z_0 = 10$ cm.

3.2. *Geostrophic wind along the coastline*

If the geostrophic wind blows parallel to the coastline, the results may not be as straightforward as in the case of an on-shore–off-shore wind. The normal-to-coast component of the ABL wind is now purely frictionally induced and, consequently, the vertical motions might be weaker. Fig. 6a shows the vertical velocity field in the quasi-steady state of the model in the case of no topography, but with roughness lengths $z_0 = 10$ cm

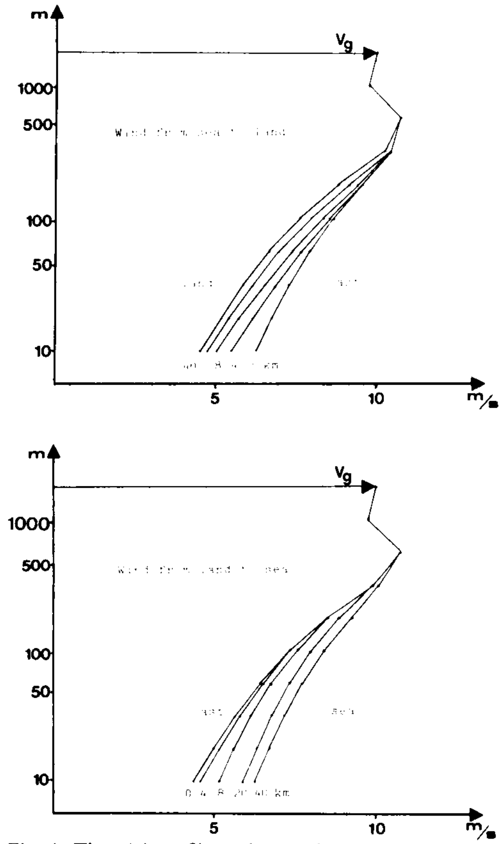

Fig. 4. The $u(z)$ profile at the steady state 0, 4, 8, 20 and 40 km downwind from the roughness change. Note the logarithmic vertical scale.

over land, 1 mm over sea, and $V_g = (0, 10)$ m s^{-1} (V_g into the paper in Fig. 6). The maximum upward motion of 0.46 cm s^{-1} occurs at around the 600 m level over the sea 25 km from the coast toward the lower pressure. A similar sinking motion region, $w = -0.38$ cm s^{-1}, is found 15 km in-land from the opposite shore line. These results are in accordance with observations that easterly upper winds in autumn and winter are more correlated with rain and cloudiness in the south coast of Finland than are westerly upper winds.

In Fig. 6a, there are also two narrow w patterns just above the coast lines. These low-level features may be traced back to the wind profiles in Fig. 2b where the v values are larger over sea than over land very near the surface, yet the cross-isobar angle is larger over land than over sea. A similar feature is also present in the Ekman–Taylor profile (Fig. 2a). This local increase of wind over sea leads to convergence and vertical motions similar to those in Fig. 3 but on a shallow layer.

When there is no roughness difference ($z_0 = 10$ cm everywhere) but slopes are included (simulating a broad, long valley), the vertical velocity extrema (not shown) occur at low levels (100–200 m) over the slopes and are small, $w = \pm 0.4$ cm s^{-1}. Including both the smooth sea and sloping coasts, the model produces the vertical velocity pattern in Fig. 6b for wind 10 m s^{-1} along the coastlines. The features are similar to Fig. 6a except that the shallow patterns over the coasts are slightly damped and the 600 m level vertical motion patterns now occur nearer to the coastlines.

In Fig. 6c, the roughness length over land is increased from 10 to 70 cm, a value used, e.g., in

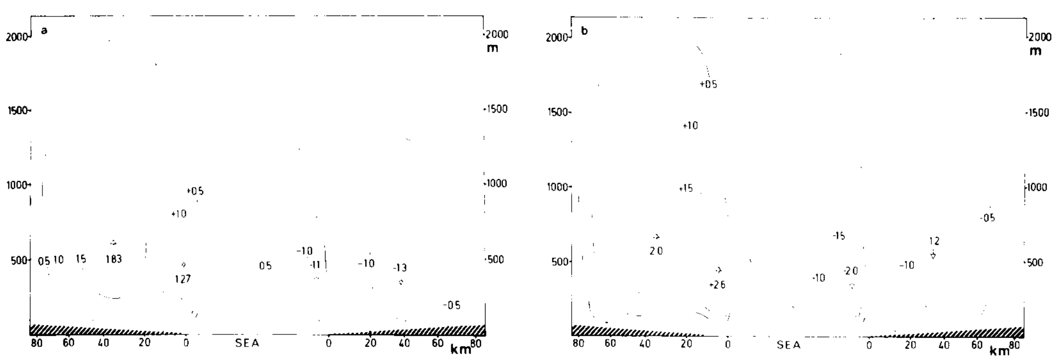

Fig. 5. Same as Fig. 3, but (a) topography is included ($z_s = 80$ m at 80 km from coasts), (b) topography is included and the land roughness length increased from 10 to 70 cm

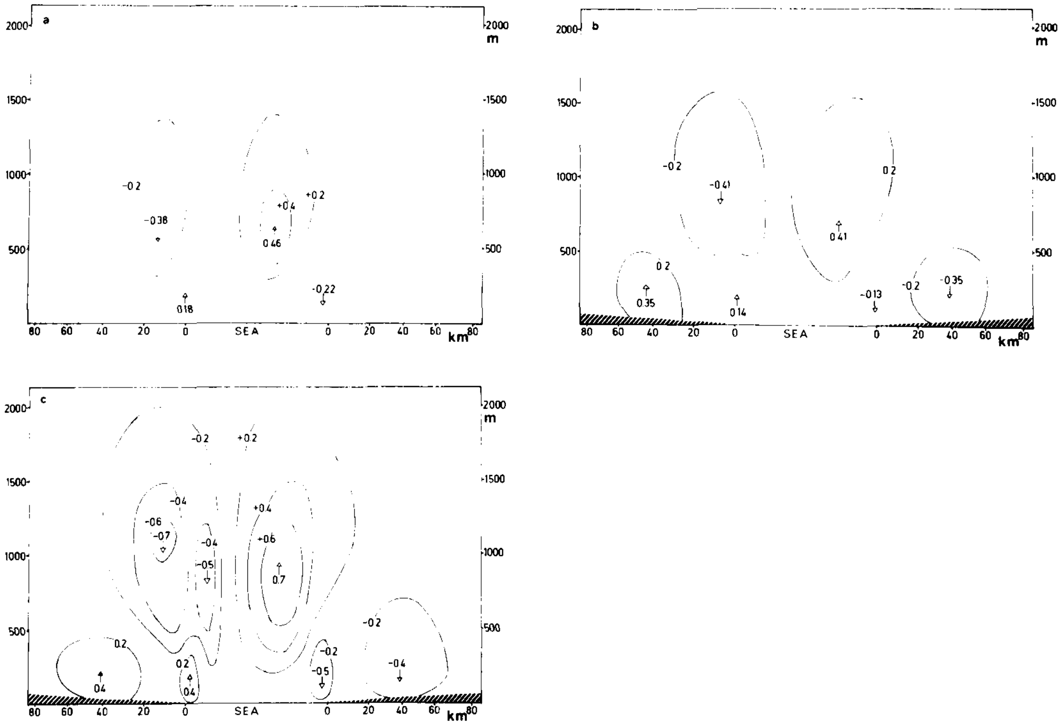

Fig. 6. Same as Fig. 3, but for transverse geostrophic wind $u_g = 0$, $v_g = 10$ m s^{-1} (into the figure): (a) land roughness length $z_0 = 10$ cm, no topography; (b) topography is included; (c) topography is included and $z_0 = 70$ cm over land.

the ECMWF model over land areas in Scandinavia. The vertical velocities due to the slope effect are increased only slightly. The coastal convergence, however, is stronger than in Fig. 6b. The extrema of w are ± 0.66 cm s^{-1} at 600–1100 m heights and are shifted 10–30 km toward the lower pressure areas from the coastlines.

Finally, let us compare Figs. 5b and 6c which differ only due to the large-scale forcing (geostrophic flow) being, respectively, perpendicular to or along the shorelines. The w patterns arise from the divergence of the frictionally *reduced* (Fig. 5b) or frictionally *induced* (Fig. 6c) u component, the profiles of which were shown in Fig. 2b.

The two figures bear a noteworthy qualitative resemblance. The differences in the respective u profiles explain the occurrence of weaker w velocities at much lower levels in Fig. 6c, compared with those in Fig. 5b. The main dissimilarity, extra vertical motions at around 900 m level in Fig. 6c, is caused by the cross-isobar wind which is larger over rough terrain than over smooth sea in the bulk of the ABL. This leads to an opposite kind of divergence pattern to that caused directly by friction (stronger deceleration over rough terrain), which is the dominating mechanism in Fig. 5b.

4. Concluding remarks

A numerical model is applied to the frictional and topographic mechanical forcing of large-scale flow over a coastal zone in a neutral atmospheric boundary layer. The purpose of the experiments was to give quantitative estimates of vertical velocities associated with land–sea roughness contrasts and forced lifting.

It was found that when the upper (geostrophic) wind 10 m s^{-1} is across the coastline, land–sea roughness length difference of two orders of magnitude and sloping of land 1 : 1000 both produce ~ 1 cm s^{-1} vertical motion, rising for on-shore wind, sinking for off-shore wind. The extrema occur at around the 600 m level just over the coast line and over the maximum slope, respectively. When the wind is along the coast line, weak upward motion ($w \sim 0.5$ cm s^{-1}) develops over that shore line where low pressure is over the sea, due to coastal convergence, and downward motion ($w \sim -0.4$ cm s^{-1}) develops inland due to the slope effect. A small downward motion region develops near the surface just over the coast line. The patterns are opposite if lower pressure is over land relative to the coast.

The results are in accordance with (precipitation and radar) observations cited in Section 1. The induced circulation does not move in the present experiments because there are no heat contrasts. Thermal contrasts, producing, e.g., sea breeze and urban heat island, will form the subject of further articles.

The model has been used here diagnostically to produce the quasi-steady-state response of a neutral ABL with fixed topography and roughness to large-scale forcing (constant geostrophic wind). Such "local wind mapping" may be considered as a useful side result in mesoscale modelling.

5. Acknowledgement

We are grateful to Professor J. Neumann and Dr. P. Alpert for providing the original model code, and many discussions.

REFERENCES

Alpert, P., Cohen, A., Doron, E. and Neumann, J. 1982. A model simulation of the summer circulation from the Eastern Mediterranean past Lake Kinneret in the Jordan Valley. *Mon. Wea. Rev. 110*, 994–1006.

Alpert, P. and Neumann, J. 1983. A simulation of Lake Michigan's winter land breeze on 7 November 1978. *Mon. Wea. Rev. 111*, 1873–1881.

Blackadar, A. K. 1962. The vertical distribution of wind and turbulent exchange in a neutral atmosphere. *J. Geophys. Res. 67*, 3095–3102.

Blackadar, A. K. 1978. High resolution models of the planetary boundary layer. *Advances in environmental and scientific engineering, Vol. 1.* Gordon and Breach, 276 pp.

Browning, K. A. 1980. Structure, mechanism and prediction of orographically-enhanced rain in Britain. In: *Orographic effects in planetary flows*, GARP Publication Series, *23*, 85–114.

Heikinheimo, M. and Puhakka, T. 1980. On the influence of the sea on rainfall patterns: preliminary results. Preprints of the 19th Conference of Radar Meteorology, April 15–18, 1980, Miami, Florida. American Meteor. Soc., Boston, Mass., 480–485.

Solantie, R. 1975. The influence of the Baltic Sea and the Gulf of Bothnia on the weather and climate of northern Europe, especially Finland, in autumn and in winter. Finnish Meteorological Institute Contributions, 70, 28 pp.

Taylor, P. A. 1969. The planetary boundary layer above a change in surface roughness. *J. Atmos. Sci. 26*, 432–440.